

Influence of Spurious Waves on the Performance of Active Absorption Systems in Oblique Waves

Andersen, Thomas Lykke; Eldrup, Mads Røge; Frigaard, Peter

Published in:
Journal of Marine Science and Engineering

DOI (link to publication from Publisher):
[10.3390/jmse8030185](https://doi.org/10.3390/jmse8030185)

Creative Commons License
CC BY 4.0

Publication date:
2020

Document Version
Publisher's PDF, also known as Version of record

[Link to publication from Aalborg University](#)

Citation for published version (APA):
Andersen, T. L., Eldrup, M. R., & Frigaard, P. (2020). Influence of Spurious Waves on the Performance of Active Absorption Systems in Oblique Waves. *Journal of Marine Science and Engineering*, 8(3), Article 185.
<https://doi.org/10.3390/jmse8030185>

General rights

Copyright and moral rights for the publications made accessible in the public portal are retained by the authors and/or other copyright owners and it is a condition of accessing publications that users recognise and abide by the legal requirements associated with these rights.

- Users may download and print one copy of any publication from the public portal for the purpose of private study or research.
- You may not further distribute the material or use it for any profit-making activity or commercial gain
- You may freely distribute the URL identifying the publication in the public portal -

Take down policy

If you believe that this document breaches copyright please contact us at vbn@aub.aau.dk providing details, and we will remove access to the work immediately and investigate your claim.

Article

Influence of Spurious Waves on the Performance of Active Absorption Systems in Oblique Waves

Thomas Lykke Andersen *, Mads Røge Eldrup and Peter Frigaard

Department of the Built Environment, Aalborg University, 9220 Aalborg Ø, Denmark;
mre@civil.aau.dk (M.R.E.); pf@civil.aau.dk (P.F.)

* Correspondence: tla@civil.aau.dk; Tel.: +45-60632203

Received: 10 February 2020; Accepted: 3 March 2020; Published: 9 March 2020

Abstract: Existing active absorption systems do not take into account the spurious waves caused by the segmentation of the wavemaker. Thus, the theoretical estimated performance curves for oblique waves are only valid for infinitely narrow segments. In the present paper, it is demonstrated that by ignoring the spurious waves, an unstable system might be designed for box-mode paddles (piecewise constant segmentation). For vertical hinged pistons (piecewise linear segmentation), the results are the opposite, as the stability of the system is improved at high frequencies when a finite paddle width is considered. It is also shown that finite discretization leads to a directional influence in the system, even for a pseudo-3D active absorption system. This effect is more pronounced for vertical hinged systems compared to box-mode paddles.

Keywords: active absorption; reflection compensation; spurious waves; directional waves; wave generation; wave basin design; wavemakers

1. Introduction

Accurate physical modelling requires in many cases to deal in a proper way with wave reflections from models or boundaries in the model testing facility. Reflected waves in wave flumes and basins will, without active absorption, be re-reflected at the wavemaker and become incident waves. The purpose of the active absorption system is to generate an opposite wave to the re-reflected one so that the two will cancel each other out.

In wave flumes, a single paddle is usually used for wavemaking, and reflected waves are usually unidirectional. Thus, active absorption systems usually assume reflected waves to be head-on to the wavemaker. Examples of such systems are Milgram [1,2], Schäffer et al. [3], and Lykke Andersen et al. [4,5] for nearfield surface elevation feedback, Frigaard and Christensen [6] and Hald and Frigaard [7] for farfield surface elevation and/or particle velocity feedback, and Salter [8], Chatry et al. [9] and Spinneken and Swan [10] for force feedback.

Even though waves in such systems are assumed to be head-on to the wavemaker, these systems are widely used in wave basins. In such cases, a number of 2-D systems are used in parallel to form a pseudo-3D system, whereby the wave direction is not taken into account, and thus, performance decreases with increasing obliqueness of the waves to be absorbed. To perfectly absorb an oblique wave, a reduced wavemaker stroke will be required, and the phase must also be slightly different. For this reason, pseudo-3D systems overreact when absorbing oblique waves, cf. Schäffer and Klopman [11].

The system by Schäffer et al. [3] was extended to a full-3D system by Schäffer [12], in which the wave direction is taken into account by including neighboring wave paddles. The Schäffer [12] system was validated in a numerical wave basin by Schäffer and Skourup [13]. The transfer function used for the full-3D system [12] is based on linear wavemaker theory for fully dispersive waves

including evanescent modes (fully linear wavemaker theory). Evanescent modes are standing waves in the nearfield caused by not generating the correct vertical velocity distribution, e.g., when using a piston wavemaker to generate a deep water wave. However, Schäffer did not take into account the spurious waves generated by the wrong longitudinal velocity distribution, which occurs due to the segmentation of the wavemaker (i.e., insufficient discretization of the wavemaker). As demonstrated by Sand [14] and also by Schäffer [15], these spurious waves might be standing waves in the nearfield, but they might also be free propagating waves with a different direction to the target free wave. Inherently Schäffer [12] thus assumed an infinitely small segment width. Schäffer and Skourup [16] mention this limitation, but its consequences were not discussed.

In the present study, the consequence of spurious waves on the performance of active absorption systems is studied. First, the mathematical model for the nearfield surface elevation without and with spurious waves is presented. Then, the equations for the theoretical absorption performance are introduced, with and without spurious waves included. Based on the developed equations, the influence of paddle discretization on the theoretical performance curve for oblique waves is quantified for typical configurations of shallow water wave basins. Finally, the consequences of the obtained results with respect to the performance and stability of active absorption systems are discussed.

2. Nearfield Surface Elevations for Infinitely Narrow Paddles

The surface elevation in the nearfield may be calculated from the Biésel far- and near-field transfer functions, cf. Biésel and Suquet [17]. The nearfield disturbance appears because the vertical velocity profile generated by the wavemaker deviates from the one in the farfield. In the present section, we only consider a linear wave generated by infinitely narrow paddles; thus, spurious waves which occur due to the segmentation of the wavemaker are not considered. Assuming the wavemaker is located along the y -axis, then Equation (2) defines the motion needed to generate a linear regular wave with the farfield surface profile given by Equation (1).

$$\eta(x, y, t) = \frac{H}{2} \cos(\omega t - k_x x - k_y y) \quad (1)$$

$$X(y, z, t) = e_0 f(z) \sin(\omega t - k_y y) \quad (2)$$

where ω is the cyclic frequency. The displacement amplitude at the still water level ($z = 0$) is $e_0 = 0.5H/C_{0,3D}$, where $C_{0,3D}$ is the farfield Biésel transfer constant for oblique waves, cf. Equation (5). $f(z)$ describes the vertical variation of the paddle displacement and is unity for piston wavemakers, while expressions for other wavemaker types are given in Lykke Andersen and Frigaard [17]. The distance between two crests along the wavemaker (y -axis) is $L_y = 2\pi/k_y = L/\sin \theta$, where L is the wavelength. Thus, $\mathbf{k} = [k_x, k_y] = k[\cos \theta, \sin \theta]$ is the wave number vector for the progressive wave. The wave number (k) is the real solution to the linear dispersion relation:

$$\omega^2 = gk \tanh(kh) \quad (3)$$

where g is the gravity acceleration and h is the water depth. In Equation (3), the surface tension and nonlinearity effects are ignored. Surface tension is important for very short waves (capillary waves), but for the frequencies examined in the present paper (0–4 Hz), the influence of surface tension on the wavelength is 3% at most. For frequencies that show the most interesting results (up to 2.5 Hz), the effect is less than 0.5% on the wavelength, and is thus, negligible. Nonlinear effects might be more important. The phenomena studied later in the paper are mainly related to the wavelength. As both amplitude dispersion and surface tension effects result in waves which are longer than those given by Equation (3), some of the observed phenomena might occur at slightly higher frequencies than what is given by the results of the present paper.

The surface elevation (η), including the nearfield disturbance generated by the displacement in Equation (2), may be calculated using linear wavemaker theory in a given coordinate (x, y) as a function of time (t) according to Lykke Andersen and Frigaard [18]:

$$\frac{\eta(x, y, t)}{e_0} = C_{0,3D} \cos(\omega t - k_x x - k_y y) + \sum_{j=1}^{\infty} C_{j,3D} \exp\left(-\sqrt{k_j^2 + k_y^2} x\right) \sin(\omega t - k_y y) \quad (4)$$

where $C_{j,3D}$ are the Biésel transfer constants which, for $j = 0$, is the farfield transfer constant and for $j > 0$ is the nearfield transfer constants (evanescent waves). The far- and near-field transfer constants for oblique waves are related to those for head-on waves through:

$$C_{0,3D} = C_{0,2D} \frac{k}{\sqrt{k^2 - k_y^2}} = \frac{C_{0,2D}}{\cos \theta} \quad (5)$$

$$C_{j,3D} = C_{j,2D} \frac{k_j}{\sqrt{k_j^2 - k_y^2}} \text{ for } j \geq 1 \quad (6)$$

The constants $C_{j,2D}$ depend on the wavemaker type and are given in Biésel and Suquet [17]. For a piston wavemaker, we have:

$$C_{0,2D} = \frac{2 \sinh^2 kh}{\sinh kh \cosh kh + kh} \quad (7)$$

$$C_{j,2D} = \frac{2 \sin^2 k_j h}{\sin k_j h \cos k_j h + k_j h} \text{ for } j \geq 1 \quad (8)$$

The wave numbers k_j for the evanescent waves ($j > 0$) might be calculated as the positive solutions to:

$$\omega^2 = -gk_j \tan(k_j h) \quad (9)$$

Equation (4) may be written as:

$$\frac{\eta(x, y, t)}{e_0} = C_{0,3D} \cos(\omega t - k_x x - k_y y) + E(x) \sin(\omega t - k_y y) \quad (10)$$

where the nearfield Biésel transfer function is given by:

$$E(x) = \sum_{j=1}^{\infty} C_{j,3D} \exp\left(-\sqrt{k_j^2 + k_y^2} x\right) \quad (11)$$

These equations are used to generate linear regular waves. Linear irregular waves are produced by generating a number of regular wave components at various frequencies and in various directions. Thus, by applying above theory for each component, irregular waves may be generated.

3. Spurious Waves

To generate waves obliquely to a wavemaker, a segmented wavemaker is needed. Due to the inability of the segmented front of the wavemaker to form the sinusoid given by Equation (2), so-called spurious waves are generated. Spurious waves are caused by the generated velocity variation along the wavemaker being different from the theoretical profile of the target farfield wave. The nearfield disturbance presented in Section 2 is due to vertical variations in the velocity being different from the target. Thus, spurious waves have a similar origin to the nearfield disturbances described in Section 2, but are caused by the wrong longitudinal distribution, as opposed to the vertical one. The wrong vertical distribution causes only a nearfield disturbance (evanescent modes), whereas the wrong longitudinal distribution may lead to both evanescent and progressive waves. If progressive spurious waves occur, they will propagate into the model area.

Spurious waves were dealt with theoretically by Sand [14] and Schäffer [15], who showed that their relevance depends on the wavelength (L), wave direction (θ), segment width (l_p) as well as on the discretization type. Typically, stepwise linear (vertical hinged) or stepwise constant (box-mode) segmented wavemakers are used (see Figure 1).

In both cases, the paddle shape deviates from the target sinusoid described by Equation (2) and spurious waves are generated. For identical segment width (l_p), the piecewise linear discretization is a much better approximation of the theoretical sinusoid. For this reason, the spurious waves are also much smaller for this segmentation than for box-mode paddles. Box-mode wavemakers are more common due to their simpler mechanical arrangement.

In order to study the influence of spurious waves on active absorption systems, it is necessary to establish a mathematical model for the surface elevation in the nearfield including spurious waves. For this purpose, we use the method outlined by Sand [14] and Schäffer [15] for infinitely long segmented wavemakers. It is desirable to work with complex notation, with $i = \sqrt{-1}$ being the imaginary unit number.

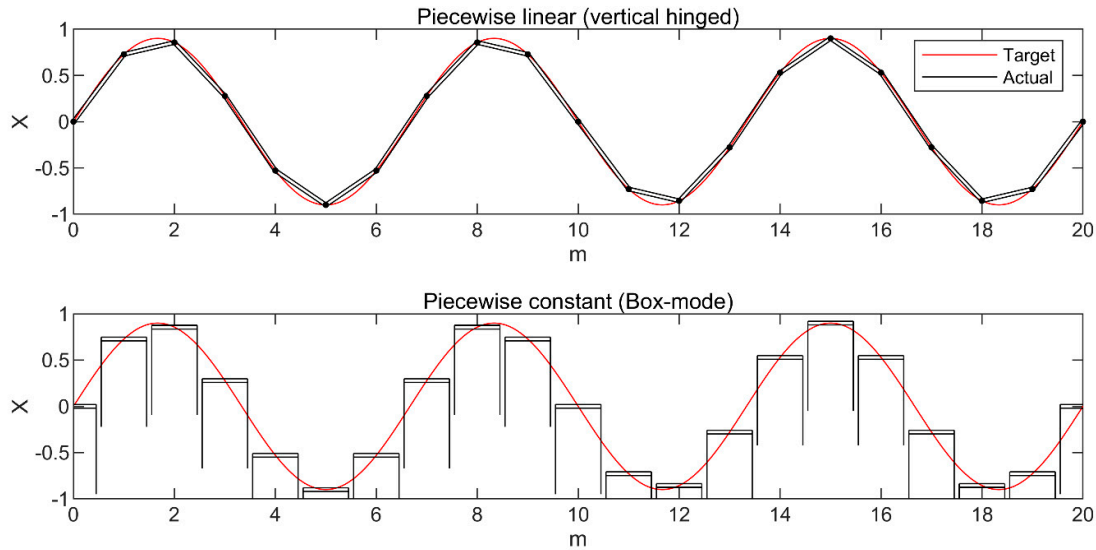


Figure 1. Example of vertical hinged and box-mode representation for a case with $l_p/L_y = 0.15$. m represents the actuator number. Actuators are thus located at $y_m = m l_p$, where l_p is the segment width.

In the actuator positions y_m , the motions perfectly follow Equation (2); using complex notation, we have:

$$X(y_m, 0, t) = \text{Re} \left\{ e_0 \exp \left(i(\omega t - k_y y_m) \right) \right\} \quad (12)$$

where $y_m = m l_p$ with m being an integer. Between the actuator positions, the paddle positions may be written as:

$$X(y, 0, t) = \text{Re} \{ \xi(y) e_0 \exp(i\omega t) \} \quad (13)$$

where $\xi(y)$ is dependent on the discretization type. At the actuator positions, we have in accordance with Equation (12) that $\xi(y_m) = \exp(-ik_y y_m)$. For box-mode paddles, we have a piecewise constant function where the paddle position for each board is equal to the position at the actuator, and is thus given by Equation (14). For vertical hinged paddles, the displacement is a piecewise linear function between two actuators, as given by Equation (15).

$$\xi(y) = k_y y_m \quad \text{for } y_m - 0.5l_p \leq y \leq y_m + 0.5l_p \quad (14)$$

$$\xi(y) = \xi(y_m) \frac{y_{m+1} - y}{l_p} + \xi(y_{m+1}) \frac{y - y_m}{l_p} \quad \text{for } y_m \leq y \leq y_{m+1} \quad (15)$$

Sand [14] and Schäffer [15] expanded $\xi(y)$ in a Fourier series, and after quite some algebra, they found:

$$\xi(y) = \sum_{p=-\infty}^{p=\infty} a_p \exp(-k_{yp}y) \quad (16)$$

where:

$$a_p = \begin{cases} \beta_p & \text{for piecewise constant (box – mode)} \\ \beta_p^2 & \text{for piecewise linear (vertical hinged)} \end{cases} \quad (17)$$

$$\beta_p = \frac{\sin \alpha_p}{\alpha_p} \quad (18)$$

$$\alpha_p = \pi \left(\frac{l_p}{L_y} - p \right) \quad (19)$$

$$k_{yp} = k_y - p \frac{2\pi}{l_p} \quad (20)$$

$p = 0$ corresponds to the desired motion that occurs for infinitely narrow paddles. $p \neq 0$ is the unwanted spurious modes that occur due to the discretization. Thus, the ideal sine shape given by Equations (2) and (12) only occurs if $a_0 = 1$ and $a_p = 0$ for $p \neq 0$. The variation of $|a_p|$ with l_p/L_y is shown in Figure 2 for the two discretization types.

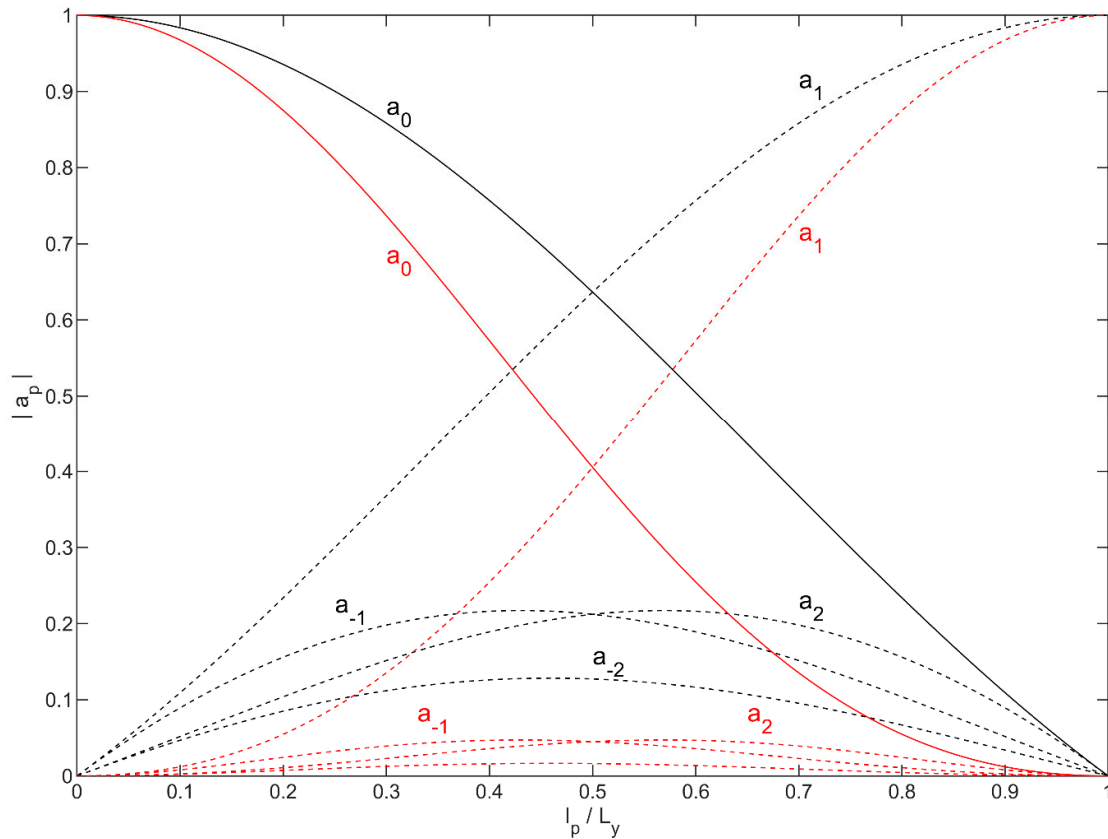


Figure 2. Amplitudes of components in Equation (16) for $p = 0, \pm 1$ and ± 2 as function of segment width (l_p) relative to the wavelength along the wavemaker ($L_y = L/\sin\theta$) for box-mode (black) and vertical hinged (red) segmentation.

It is demonstrated by Figure 2, that by increasing l_p/L_y , the amplitude of the desired motion (a_0) decreases, and the amplitude of the spurious components increases. At small values of l_p/L_y , the

amplitudes of the spurious modes vanish for vertical hinged systems while they grow linearly with l_p/L_y for box-mode systems. At $l_p/L_y = 0.5$ (the Nyquist limit), the amplitude of the first spurious component ($p = 1$) is the same as the amplitude of the desired motion, independent of the discretization type. The amplitude of the other spurious components is at the Nyquist frequency though much higher for box-mode than for vertical hinged systems. At $l_p/L_y = 1$, all paddles move in phase and only head-on waves are generated; thus, no energy is introduced in the desired motion (only spurious waves generated). The overall conclusion is that vertical hinged paddles have much less spurious energy than box-mode systems.

It is also interesting to note that the decrease of $|a_0|$ with l_p/L_y is stronger for vertical hinged systems than for box-mode systems. This is because for vertical hinged systems, less energy is introduced, as is also shown in Figure 1. In wave generation, this can be compensated for, so the desired progressive wave has the desired amplitude. The decrease in a_0 will also affect the active absorption of oblique waves, as will be shown later.

4. Nearfield Surface Elevations Including Spurious Waves

The nearfield surface elevation caused by the motion given by Equations (13)–(20) may be calculated using linear wavemaker theory for each mode (p) in Equation (16). In order to make a comparison with Equation (10), it is written in real notation, yielding:

$$\begin{aligned} \frac{\eta(x, y, t)}{e_0} = & \sum_{p=-\infty}^{\infty} C_{0,3D}(1 - \gamma) \cos\left(\omega t - \sqrt{k^2 - k_{yp}^2} x - k_{yp} y\right) \\ & + \sum_{p=-\infty}^{\infty} C_{0p,3D} \gamma \exp\left(-\sqrt{k_{yp}^2 - k^2} x\right) \sin(\omega t - k_{yp} y) + \sum_{p=-\infty}^{\infty} E_p(x) \sin(\omega t - k_{yp} y) \end{aligned} \quad (21)$$

where the first term is progressive waves (the desired one for $p = 0$ and otherwise spurious). Progressive spurious waves exist when $\gamma = 0$ and $p \neq 0$, where γ is defined as:

$$\gamma = \begin{cases} 0 & \text{for } |k_{yp}| < k \\ 1 & \text{for } |k_{yp}| \geq k \end{cases} \quad (22)$$

The second term in Equation (21) is evanescent spurious waves and the last term is the evanescent modes due to the incorrect vertical velocity profile, as described in Section 2 (for each of the p modes). The following definitions are used in Equation (21):

$$C_{0p,3D} = a_p C_{0,2D} \frac{k}{\sqrt{|k^2 - k_{yp}^2|}} \quad (23)$$

$$C_{jp,3D} = a_p C_{j,2D} \frac{k_j}{\sqrt{k_j^2 - k_{yp}^2}} \text{ for } j \geq 1 \quad (24)$$

$$E_p(x) = \sum_{j=1}^{\infty} C_{jp,3D} \exp\left(-\sqrt{k_j^2 - k_{yp}^2} x\right) \quad (25)$$

For active absorption, it is only necessary to evaluate Equation (21) at the gauge positions, which means usually only at $y = y_m$, and thus:

$$k_{yp} y_m = \left(k_y - p \frac{2\pi}{l_p}\right) y_m = k_y y_m - p \frac{2\pi}{l_p} m l_p = k_y y_m + p m 2\pi \quad (26)$$

The last term is a multiple of 2π , and thus, $k_{yp} y_m$ inside the sines and cosines can be replaced by $k_y y_m$. The extension of Equation (21) to irregular and short-crested waves is obtained by applying Equation (21) to each individual component, as discussed in Section 2.

5. Nearfield Active Absorption Theory

In the present section, the target transfer function for perfect absorption of oblique waves for infinitely narrow paddle will be given first. This is based on fully linear wavemaker theory, including evanescent modes, as also used by Schäffer [12]. Compared to Schäffer [12], however, the present transfer function is extended to also cover cases where the wave gauge is mounted with a small gap to the paddle face, as also done by Lykke Andersen et al. [5] for head-on waves.

Afterwards, the filter design method is outlined, followed by the method to calculate the theoretical re-reflection coefficient of the paddle as a function of frequency and direction for the designed filter. Compared to previous studies, these formulae will be extended to include the spurious waves based on the mathematical description given in Section 4.

5.1. Active Absorption Theory

From Equations (2) and (10), it can be seen that the following relation applies in Fourier space in case of no reflection:

$$A_{WG,Gen} = \alpha X_{Gen} \quad (27)$$

$$\alpha = -iC_{0,3D} \exp(ik_x d_{WG}) + E(d_{WG}) \quad (28)$$

where X_{gen} is the paddle position at $z = 0$. $A_{WG,Gen}$ is the surface elevation in Fourier space measured by the wave gauge (WG) located at $(x,y) = (d_{WG}, y_m)$, i.e., with a gap d_{WG} between the paddle and the wave gauge. Using this equation, it is possible to calculate the expected surface elevation at the wave gauge without reflections and active absorption.

In the present paper, a dual mode active absorption system is considered, so the generation and absorption loops are separated. Thus, the generation may be nonlinear, and only the absorption correction is based on linear wavemaker theory, as given in Equations (27)–(28). Thus, the active absorption will only react to the difference between the measured surface elevation and that which occurs due to the generated incident waves that may be calculated with nonlinear theory. In Fourier space we have:

$$A_{WG,Abs} = A_{WG,Meas} - A_{WG,Gen} \quad (29)$$

A reflected wave with a complex amplitude at the paddle A_R and a re-reflected with complex amplitude A_{RR} is now included; paddle displacement correction (X_{Abs}), that these conditions lead to, is also included. When components due to X_{Gen} are removed, this gives a surface elevation at the wave gauge:

$$A_{WG,Abs} = \alpha X_{abs} + A_R \exp(-ik_x d_{WG}) + A_{RR} \exp(ik_x d_{WG}) \quad (30)$$

Assuming 100% reflection at the paddle, then $A_{RR} = A_R$, and thus:

$$A_{WG,Abs} = \alpha X_{Abs} + 2 \cos(k_x d_{WG}) A_R \quad (31)$$

The incident farfield waves at the paddle (A_I) include the farfield components generated due to the paddle motion and the re-reflections at the paddle ($A_{RR} = A_R$). Due to dual mode system, only the generated waves due to active absorption correction should be included:

$$A_{I,Abs} = -iC_{0,3D} X_{Abs} + A_R \quad (32)$$

Isolating A_R and inserting it into Equation (31) after setting $A_{I,Abs} = 0$ for perfect active absorption gives:

$$X_{Abs} = -A_{WG,Abs} H(f, \theta) \quad (33)$$

$$H(f, \theta) = \frac{1}{iC_{0,3D} [\exp(ik_x d_{WG}) - 2 \cos(k_x d_{WG})] - E(d_{WG})} \quad (34)$$

Thus, the theoretical transfer function as a function of frequency and wave direction has been derived.

5.2. Realtime Realisation

In order to apply the transfer function in a real time system, a causal filter (digital or analogue) is needed. Due to the causality requirement of the system, the filter design is far from trivial, and only suboptimal filters may be designed. Thus, the real filter response $\tilde{H}(f, \theta)$ will be different from the target $H(f, \theta)$. The dependency of the wave direction may be included by using a 2-D filter for each paddle, as used by Schäffer [12], i.e., the response of the considered paddle depends also on the surface elevations measured on one or more neighboring paddles.

In the present case, a pseudo-3D system is used, and thus, a 1-D filter is applied for each paddle. The filter response is thus independent of θ , and the filter response is given by $\tilde{H}(f)$. Lykke Andersen et al. [5] showed that with an iterative procedure, it is possible to develop a FIR filter with slightly better performance for head-on waves than the IIR filter developed by Schäffer [12]. By using a FIR filter, error accumulation in the filter is avoided. Examples of filter designs and related performances were presented by Lykke Andersen et al. [5] for head-on waves. In the following subsection, it will be shown how the performance is calculated for oblique waves.

5.3. Theoretical Performance Curve

When a causal filter has been designed with frequency response function $\tilde{H}(f)$, the theoretical re-reflection coefficient of the paddle can be calculated based on linear wavemaker theory. In the present and following subsections, the method will be outlined both when spurious waves are excluded and included.

The active absorption paddle correction signal \tilde{X}_{abs} from $\tilde{H}(f)$ is found by inserting Equation (31) into Equation (33):

$$\tilde{X}_{Abs} = -[\alpha \tilde{X}_{Abs} + 2 \cos(k_x d_{WG}) A_R] \tilde{H}(f) \quad (35)$$

which can be rearranged into:

$$\tilde{X}_{Abs} = -\frac{2A_R \cos(k_x d_{WG})}{1/\tilde{H}(f) + \alpha} \quad (36)$$

The re-reflection coefficient of the paddle is defined as the re-reflected amplitude divided by the amplitude of the wave to be absorbed (the reflected wave). The re-reflected amplitude is the sum of the generated incident waves from the absorption correction \tilde{X}_{abs} and $A_{RR} = A_R$. For infinitely narrow paddles, the re-reflected amplitude becomes:

$$\tilde{A}_{I,abs} = -iC_{0,3D} \tilde{X}_{abs} + A_R \quad (37)$$

By including \tilde{X}_{abs} from Equation (36) and rewriting, the following is found:

$$-\frac{\tilde{A}_{I,abs} - A_R}{A_R} = -\frac{i2C_{0,3D} \cos(k_x d_{WG})}{1/\tilde{H}(f) + \alpha} \quad (38)$$

where the right hand side is the performance parameter $\lambda(f, \theta)$. Thus, we get the following equation to calculate the reflection coefficient:

$$C_r(f, \theta) = \left| \frac{\tilde{A}_{I,abs}}{A_R} \right| = \left| 1 + \frac{\tilde{A}_{I,abs} - A_R}{A_R} \right| = |1 - \lambda(f, \theta)| \quad (39)$$

The re-reflection coefficient can thus be calculated by Equation (39), where for infinitely narrow paddles, the performance parameter λ is calculated from:

$$\lambda(f, \theta) = -\frac{i2C_{0,3D} \cos(k_x d_{WG})}{1/\tilde{H}(f) + \alpha} \quad (40)$$

$$\alpha = -iC_{0,3D} \exp(ik_x d_{WG}) + E(d_{WG}) \quad (41)$$

5.4. Theoretical Performance Curve Including Spurious Waves

For finite paddle segment width, spurious waves occur, causing two changes to the equation presented above. The function α that relates the paddle displacement to the nearfield surface elevation (see Equation (27)) is changed in accordance with Equation (21). This is the only change in the function of \tilde{X}_{abs} in Equation (36). Furthermore, Equation (37) is changed, as it is seen that the incident waves due to absorption correction in the direction of the re-reflected waves are found for $p = 0$ only. Thus, Equation (37) becomes:

$$\tilde{A}_{I,abs} = -iC_{00,3D}\tilde{X}_{abs} + A_R \quad (42)$$

The paddle re-reflection coefficient can thus be calculated from Equation (39) for $p = 0$ using the following parameters:

$$\lambda(f, \theta) = -\frac{i2C_{00,3D} \cos(k_x d_{WG})}{1/\tilde{H}(f) + \alpha} \quad (43)$$

$$\alpha = -i \sum_{p=-\infty}^{\infty} C_{0p,3D}(1-\gamma) \cos\left(\sqrt{k^2 - k_{yp}^2} d_{WG}\right) + \sum_{p=-\infty}^{p=\infty} \left[E_p(d_{WG})C_{0p,3D}(1-\gamma) \sin\left(\sqrt{k^2 - k_{yp}^2} d_{WG}\right) + C_{0p,3D}\gamma \exp\left(-\sqrt{k_{yp}^2 - k^2} d_{WG}\right) \right] \quad (44)$$

The above relation for α is determined using Equation (21), remembering that Equation (26) applies for the wave gauge positions assuming gauges located at $y = y_m$.

5.5. Reflections in Other Directions Due to Spurious Waves

Above, we only considered the direction of the re-reflected waves, but the absorption correction might lead to unwanted waves in other directions being generated due to spurious waves being generated during the absorption of the reflected waves. The spurious waves are progressive for $|k_{yp}| < k$. As shown in Figure 2, the spurious waves might be high, and thus it cannot be ruled out that re-reflections in other directions may be higher than in the direction of the re-reflected wave. Waves in other directions occur for $p \neq 0$ when the p value corresponds to a progressive wave. In that case, they lead to an additional re-reflection being generated with amplitude:

$$\tilde{A}_{I,abs} = -iC_{0p,3D}\tilde{X}_{abs} \quad \text{for } p \neq 0 \text{ and } |k_{yp}| < k \quad (45)$$

The re-reflection caused in other directions ($p \neq 0$) is found by inserting \tilde{X}_{abs} from Equation (36) into the above, which gives:

$$C_r(f, \theta) = \left| \frac{\tilde{A}_{I,abs}}{A_R} \right| = |-\lambda(f, \theta)| \quad (46)$$

$$\lambda(f, \theta) = \begin{cases} -\frac{i2C_{0p,3D} \cos(k_x d_{WG})}{1/\tilde{H}(f) + \alpha} & \text{for } |k_{yp}| < k \\ 0 & \text{for } |k_{yp}| \geq k \end{cases} \quad (47)$$

where α is given by Equation (44). Thus, both the reflection in the direction of the re-reflected wave and in the direction of the progressive spurious waves are studied in the following section.

6. Results

In order to demonstrate the influence of the spurious waves on the performance and stability of the pseudo-3D active absorption system, a typical shallow water basin with water depth $h = 0.65$ m is considered. Such a basin typically uses a segmented piston wavemaker with a segment width of around half a meter; for this reason, we consider piston wavemakers with $l_p = 0.5$ m. The control delay used is 40 ms, which is a typical value for control systems with low delay (VTI for example). As the

control delay is low, the wave gauge can be flush mounted ($d_{wg} = 0$) with good absorption performance for head-on waves. Lykke Andersen et al. (2016) demonstrated less than 10% reflection in a wide frequency range. The frequency band in which the system performance is optimized is, in the present case, from 0.15 Hz to 1.2 Hz. The filter has 3281 filter coefficients at a 50 Hz sample frequency, corresponding to a duration of around 65 s. The long filter length makes it possible to absorb long waves with a FIR filter.

6.1. Re-Reflection Coefficient in the Direction of the Re-Reflected Wave ($p = 0$)

Using Equation (39), the theoretical performance curves for the re-reflection in the direction of the re-reflected wave are calculated and given in Figure 3 for the case with $d_{wg} = 0$. Performance curves are given for infinitely narrow paddles (Equations (39)–(41)), as well as vertical hinged and box-mode segmented wavemakers (Equations (39), (43), and (44)). It appears that from 1.25 Hz and beyond, there are peaks and jumps in the paddle re-reflection coefficients caused by spurious waves. A closer examination reveals that the jumps occur when the spurious wave components change from being evanescent ($\gamma = 1$) to progressive ($\gamma = 0$). This transition occurs for a given mode (p) of the spurious waves when $|k_{yp}| = k$. Table 1 shows the frequencies where this is fulfilled for various values of p for the present case (i.e., $l_p = 0.5$ m and $h = 0.65$ m) and the directions considered in Figure 3.

Table 1. Frequencies in hertz where spurious waves transit from evanescent to progressive.

| Spurious Mode | $\theta = 20^\circ$ | $\theta = 40^\circ$ | $\theta = 60^\circ$ | $\theta = 80^\circ$ |
|---------------|---------------------|---------------------|---------------------|---------------------|
| $p = +1$ | 1.525 | 1.379 | 1.293 | 1.254 |
| $p = +2$ | 2.157 | 1.950 | 1.829 | 1.774 |
| $p = +3$ | 2.642 | 2.388 | 2.241 | 2.173 |
| $p = +4$ | 3.051 | 2.757 | 2.587 | 2.509 |
| $p = +5$ | 3.411 | 3.083 | 2.893 | 2.805 |
| $p = -1$ | 2.178 | 2.957 | 4.828 | 14.337 |
| $p = -2$ | 3.081 | 4.181 | 6.828 | 20.275 |

It is also clear from Figure 3 that box-mode paddles might have significant stability issues as the paddle re-reflection coefficient exceeds unity significantly for highly oblique waves and peaks at $C_r = 2.5$ at $f = 2.2$ Hz. Both the vertical hinged system and the infinitely narrow paddles have re-reflection coefficients which are below unity at every frequency and wave direction combination. This reveals the importance of considering spurious waves in stability assessments of active absorption systems with box-mode paddles.

One might think that stability issues can be avoided by only introducing energy at frequencies below the limit where stability issues can occur. However, this does not solve the problem, as energy at higher frequencies is generated in the model area due to wave nonlinearities, wave-structure interactions, and wave breaking. Also, electrical noise in the signals might occur at the problematic frequencies. In both cases, the result is the introduction of energy at the problematic frequencies that might grow over time, and might even lead to an unstable system. It should be noted that most control systems (e.g., PID controllers) attenuate higher frequencies to some extent, and thus, reduce somewhat the stability issues presented in Figure 3. With respect to the performance inside the operational frequency band, it can be seen that from 0.8–1.2 Hz, the performance of the vertical hinged system is notably better than for infinitely narrow paddles. For box-mode paddles, the same effect is observed, but to lesser degree. This directional dependency for segmented wavemakers is caused by the generated amplitude of the target wave ($p = 0$) is decreasing when l_p/L_y increases (see Figure 2). For this reason, the effect is most pronounced at higher frequencies (low values of L_y). For vertical hinged system, the effect is more pronounced than for box-mode systems (see variation of a_0 in Figure 2). For this reason, there is some directional dependency, even in a pseudo-3D system, but it is only significant in a small part of the operational frequency band.

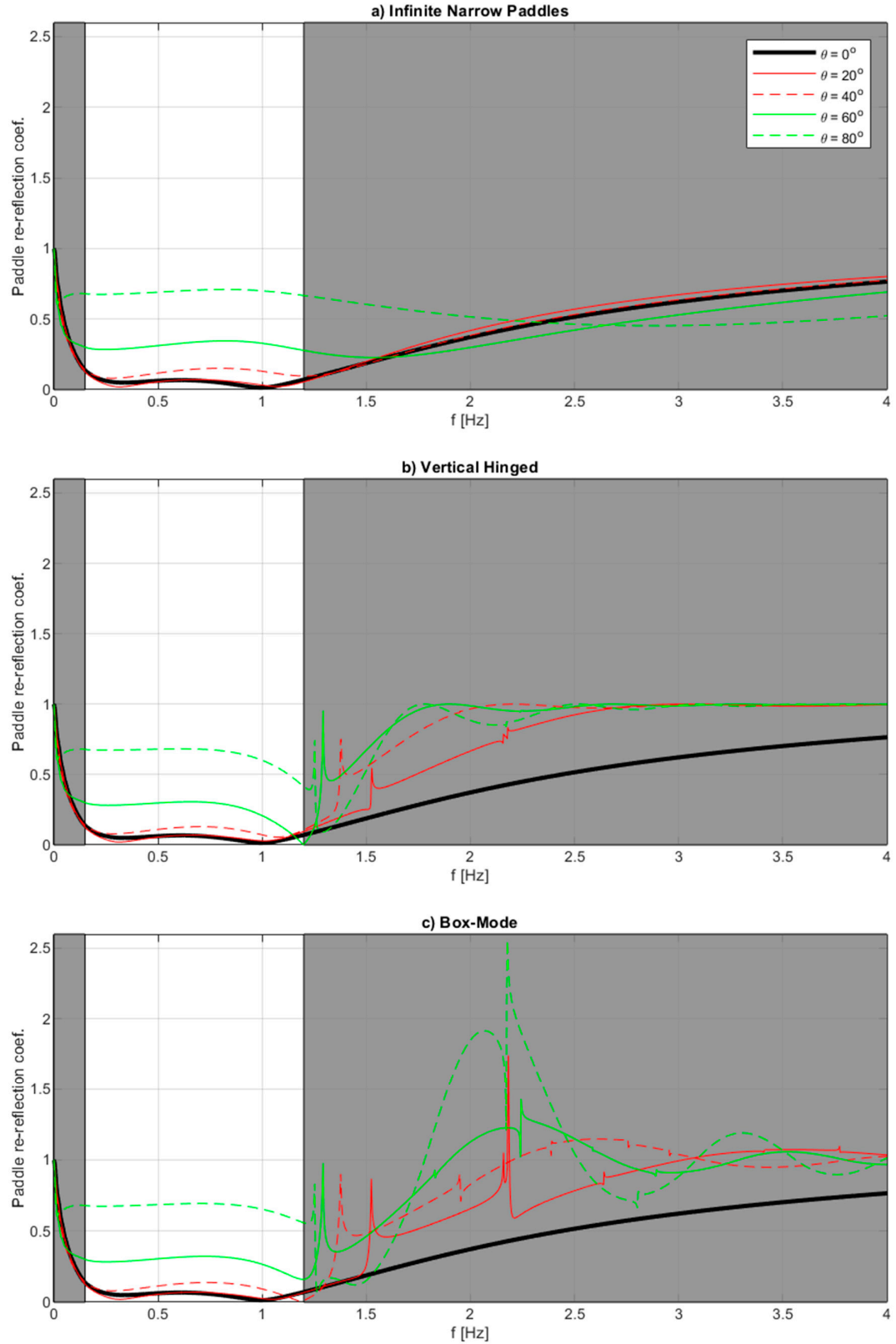


Figure 3. Performance curves in terms of paddle re-reflection coefficient as a function of frequency and obliquity of the wave to be absorbed. Example for a water depth of $h = 0.65$ m and flush mounted gauges ($d_{wg} = 0$). (a) Infinitely narrow paddles; (b) Vertical hinged pistons with segment widths of $l_p = 0.5$ m.; (c) Box-mode pistons also with $l_p = 0.5$ m.

It appears that even though only pseudo-3D systems are used, the performance is excellent up to 40 degree obliquity with less than 13% reflection in the tuned frequency range from 0.15 to 1.2 Hz. For 60 degree obliquity, the reflection shows a maximum of around 30% re-reflection in the same band.

Vertical hinged paddles with flushed mounted gauges ($d_{wg} = 0$) are mechanically difficult to manufacture, as it is assumed that the gauges will be mounted in front of the hinge ($y = y_m$). In practice, a small gap is needed, and we thus also consider a case with $d_{wg} = 3$ cm, with the remaining parameters being identical. As the transfer function is different, the filter is also recalculated. The results for this configuration are shown in Figure 4. In this case, the theoretical phase at higher frequencies has jumps which make it difficult to avoid paddle re-reflection coefficients above 1.0 for head-on waves at every frequency. In the present example, the maximum re-reflection coefficient appears at 4.3 Hz with a re-reflection coefficient $C_r = 1.10$. This small exceedance of unity has, however, not posed any stability issues, even for control systems that do not attenuate higher frequencies. Otherwise, the small gap ($d_{wg} = 3$ cm) has only minor influence on the obtained results for both box-mode and vertical hinged systems. Nevertheless, it is worth restating that Lykke Andersen et al. [5] showed that a small gap may be used to improve performance in cases where the control system has a larger delay (i.e., above 80–100 ms).

6.2. Re-Reflection Coefficient in Other Directions ($p \neq 0$)

Using Equation (46), the theoretical performance curves for the re-reflection in other directions than the re-reflected wave are calculated for the case with $d_{wg} = 0$. Performance curves are given in Figure 5 for vertical hinged and box-mode segmented wavemakers (Equations (44), (46), and (47)). Only the p value with the highest re-reflection coefficient is presented in Figure 5.

The figure shows that for vertical hinged paddles, the re-reflection coefficient in other directions than the re-reflected wave ($p \neq 0$) only slightly exceeds unity and only in a very narrow frequency band around the singularity for $p = 1$, and only for high obliquity of the incoming wave to be absorbed.

For box-mode systems, very high re-reflection coefficients are found for many p -values ($p \neq 0$) around the singularities. However, as the very high re-reflection coefficient occurs in a narrow frequency band, it might not cause major stability issues, as amplitude dispersion is expected to set an upper limit to the growth of the energy at these singularities. The main stability issues are expected to be those caused in the direction of the re-reflected wave, as discussed in the previous section, where the re-reflection coefficient exceeded unity in a wider frequency band. However, it cannot be ruled out that for box-mode systems, re-reflections in other directions might also lead to stability issues.

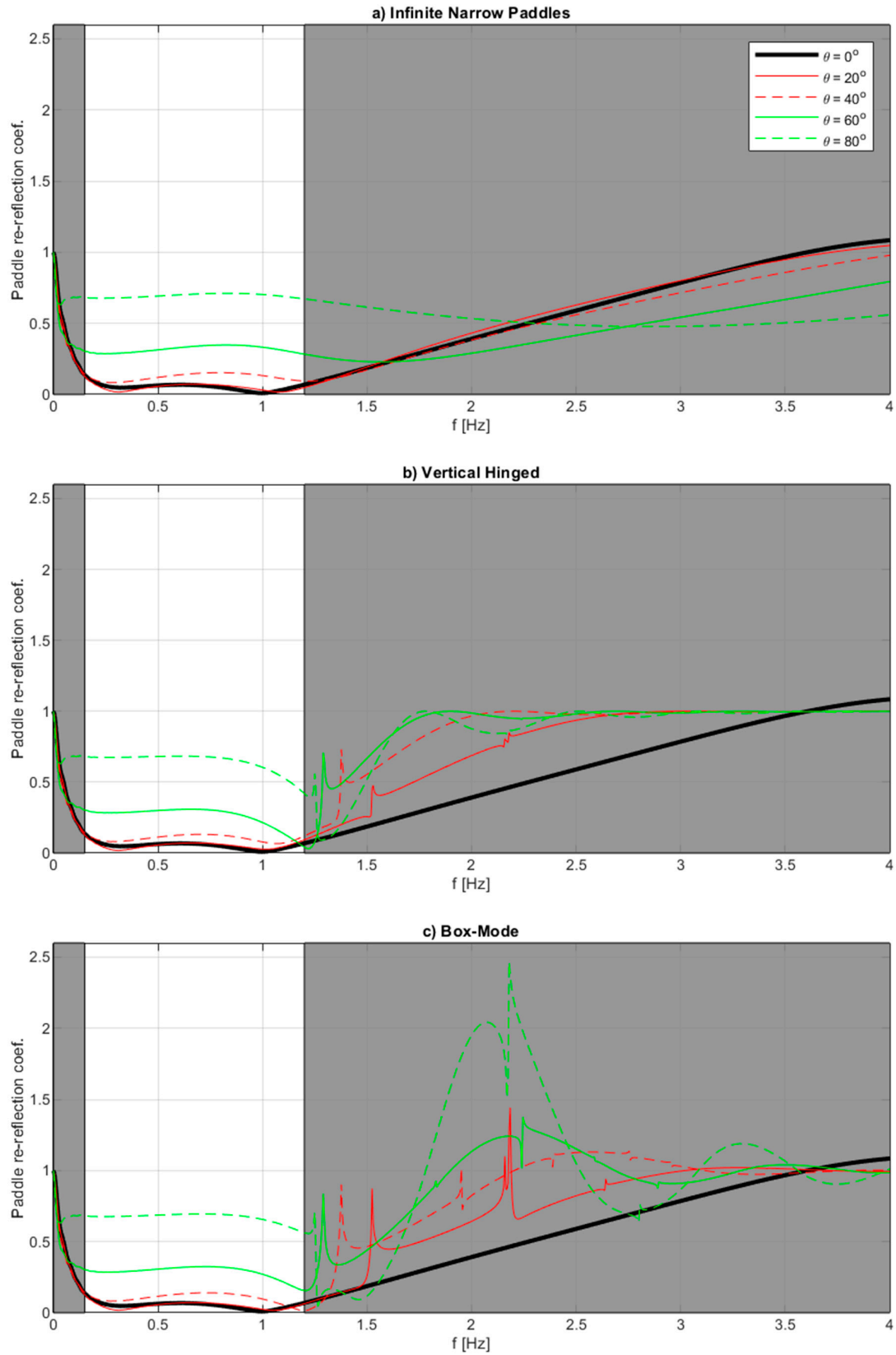


Figure 4. Same as Figure 3 but for wave gauges with a small gap to the paddle face ($d_{wg} = 3$ cm).

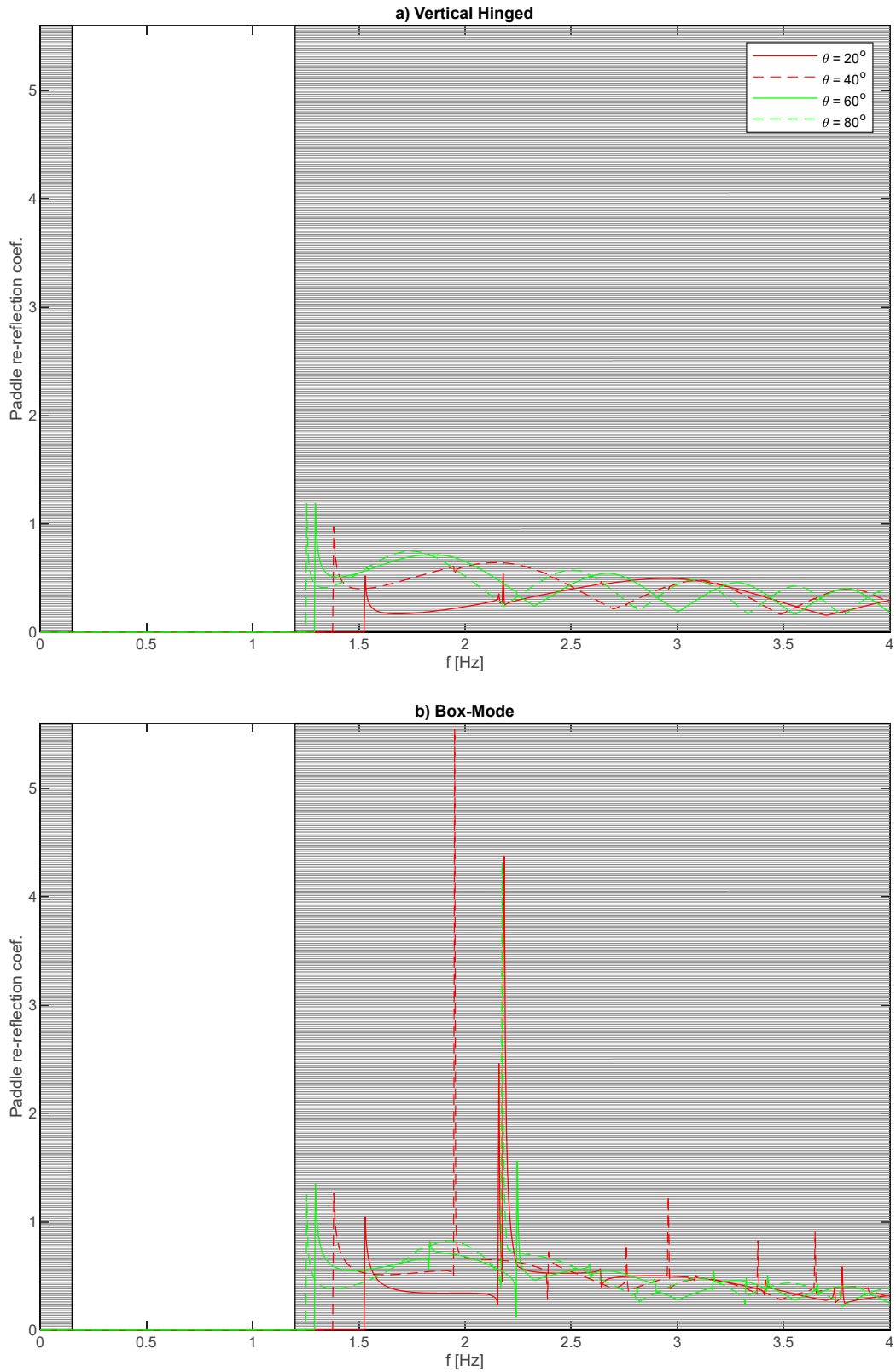


Figure 5. Performance curves in terms of paddle reflection coefficient for the p -value different from unity leading to the highest reflection as a function of frequency and obliquity of the wave to be absorbed. The case is identical to that studied in Figure 3. (a) Vertical hinged pistons with segment widths of $l_p = 0.5$ m.; (b) Box-mode pistons also with $l_p = 0.5$ m.

7. Discussion

Short-crested waves in laboratories are generated by summing a number of components with various directions. A segmented wavemaker may be used to generate and absorb waves from many directions simultaneously. Generating a single oblique wave component in the laboratory means that the wavemaker front should form a sinusoid. Segmented wavemakers are most typically discretized with stepwise constant approximation (box-mode paddles) or stepwise linear approximation (vertical hinged paddles). When generating oblique waves with a segmented wavemaker using the aforementioned approximations, spurious waves cannot be avoided. This is because the wavemaker is unable to form the theoretical sinusoid. For identical segment widths, spurious waves are much higher with box-mode paddles than with vertically hinged paddles.

Active wave absorption at the wavemaker is used to absorb reflections from models or boundaries in the wave basin. When designing nearfield active absorption systems, the absorption performance is maximized in a defined frequency and direction range, but also taking into account that the system at every frequency should be stable. Previous studies ignored spurious waves when they derived the theoretical performance and stability of active absorption systems. The influence of this choice is studied in the present paper.

By utilizing the existing methodology to calculate nearfield surface elevation including spurious waves, the methodology to calculate the theoretical performance of active absorption systems for segmented wavemakers including spurious waves is given. The obtained results demonstrate that ignoring spurious waves in stability estimations of active absorption systems with box-mode paddles is very unsafe for oblique waves. In fact, unstable systems might easily be designed.

The theoretical derivations made herein were based on monochromatic linear waves generated by an infinitely long segmented wavemaker. Short-crested waves are multichromatic, and thus, each component in the sea states will behave as predicted in the present paper; thus, stability issues are exactly the same in that case. Wavemakers in wave basins are not infinitely long, but are truncated; thus, the above findings will depend on the wavemaker length and the reflectiveness of the basin boundaries and models. Stability issues are important, even though they occur outside the frequency band where the main energy exists. This is because even though no first order energy is generated by the wavemaker at such high frequencies, they will occur regardless, due to superharmonic interactions or interactions with structures. Remember also that active absorption filters are designed with an attenuation at higher frequencies. The attenuation can, however, not be too steep, as that would cause significant phase disturbances. Thus, depending on the basin configuration, even a small amount of unwanted energy might build up over time and lead to an unstable system. Energy might also be introduced at the problematic frequencies due to electrical noise in the wave gauge signals.

If energy builds up at certain frequencies, the waves become nonlinear, which might set an upper limit on the built-up energy. Thus, future work is needed to study the phenomena presented in a nonlinear numerical model or in a physical model with a truncated wavemaker.

Author Contributions: T.L.A. defined the study, developed the methodology and implemented the method in AwaSys. T.L.A. performed the case study and drafted the manuscript. The work was discussed with M.R.E. and P.F. All authors have read and agreed to the published version of the manuscript.

Funding: This research received no external funding.

Conflicts of Interest: The authors declare no conflict of interest.

References

1. Milgram, J.H. Compliant Water Wave Absorbers, Massachusetts Institute of Technology. Ph.D. Thesis, Department of Naval Architecture and Marine Engineering, Massachusetts, USA. Research Report No. 65–13, 1965.
2. Milgram, J.H. Active water-wave absorbers. *J. Fluid Mech.* **1970**, *43*, 845–859.

3. Schäffer, H.; Stolborg, T.; Hyllested, P. Simultaneous generation and active absorption of waves in flumes. In Proceedings of the Waves—Physical and Numerical Modelling, Vancouver, BC, Canada, 21–24 August, 1994; Volume 1, pp. 90–99.
4. Lykke Andersen, T.; Clavero, M.; Eldrup, M.R.; Frigaard, P.; Losada, M. Active absorption of nonlinear irregular waves. In Proceedings of the 36th International Conference on Coastal Engineering (ICCE), Baltimore, MD, USA, 30 July – 3 August, 2018.
5. Lykke Andersen, T.; Clavero, M.; Frigaard, P.; Losada, M.; Puyol, J.I. A new active absorption system and its performance to linear and non-linear waves. *Coast. Eng.* **2016**, *114*, 47–60.
6. Frigaard, P.; Christensen, M. Absorbing wave-maker based on digital filters. In Proceedings of the 24th International Conference on Coastal Engineering, Kobe, Japan, 23–28 October, 1994.
7. Hald, T.; Frigaard, P. Performance of active wave absorption systems: Comparison of wave gauge and velocity meter based systems. In Proceedings of the 7th International Offshore and Polar Engineering Conference, ISOPE, Honolulu, HI, USA, 25–30 May, 1997.
8. Salter, S.H. Absorbing wave-makers and wide tanks. In Proceedings of the Directional Wave Spectra Applications, Berkeley, CA, USA, 14–18 September, 1981; pp. 185–202. ASCE, New York, USA, 1982.
9. Chatry, G.; Clement, A.H.; Gouraud, T. Self-adaptive control of a piston wave absorber. In Proceedings of the International Offshore and Polar Engineering Conference, Montreal, QC, Canada, 24–29 May 1998; pp. 127–133. International Society of Offshore and Polar Engineers, 1998.
10. Spinneken, J.; Swan, C. Wave generation and absorption using force-controlled wave machines. In Proceedings of the 19th International Offshore and Polar Engineering Conference, Osaka, Japan, 21–26 July 2009; International Society of Offshore and Polar Engineers, 2009.
11. Schäffer, H.A. and Klopman, G., 2000. Review of multidirectional active wave absorption methods. *Journal of waterway, port, coastal, and ocean engineering*, 126(2), pp.88–97.”
12. Schäffer, H.A. Active wave absorption in flumes and 3D basins. In Proceedings of the Waves '01: Proceedings 4th International Symposium on Ocean Wave Measurement and Analysis, San Francisco, CA, USA, 2–6 September 2001; ASCE: San Francisco, CA, USA, 2001; pp. 1200–1208.
13. Skourup, J.; Schaffer, H.A. Wave generation and active absorption in a numerical wave flume. In Proceedings of the 7th International Offshore and Polar Engineering Conference, Honolulu, HI, USA, 25–30 May, 1997. International Society of Offshore and Polar Engineers, 1997.
14. Sand, S. Three-Dimensional Deterministic Structure of Ocean Waves. Ph.D. Thesis, Technical University of Denmark, Institute of Hydrodynamics and Hydraulic Engineering, Series Paper No. 24, 1979.
15. Schaffer, H.A. Some design aspects of an absorbing 3D wavemaker. In Proceedings of the 26th International Conference on Coastal Engineering, Copenhagen, Denmark, 22–26 June, 1998. ASCE, 1999.
16. Schaffer, H.A.; Skourup, J. Active absorption of multidirectional waves. In Proceedings of the 25th International Conference on Coastal Engineering, Orlando, FL, USA, 2–6 September, 1996. ASCE, 1997, pp. 55–66.
17. Biéssel, F.; Suquet, F. Les appareils générateurs de houle en laboratoire. *La Houille Blanche* **1951**, *6*, pp. 147–165.
18. Lykke Andersen, T.; Frigaard, P. *Wave Generation in Physical Models-Technical Documentation for AwaSys 6*; DCE Lecture Notes vol. 34; Department of Civil Engineering, Aalborg University: Aalborg, Denmark, 2014.

